ELSEVIER

Journal of Molecular Catalysis A: Chemical 171 (2001) 229–241

JOURNAL OF MOLECULAR CATALYSIS A: CHEMICAL

www.elsevier.com/locate/molcata

Synthesis, characterization and catalytic activity of actinide Th-MCM-41 and U-MCM-41 hexagonal packed mesoporous molecular sieves

Rodica Tismaneanu [a], Biswajit Ray [a], Rafael Khalfin [b], Rafi Semiat [b], Moris S. Eisen [a,*]

[a] *Department of Chemistry and Institute of Catalysis Science and Technology, and the Water Research Institute, Technion — Israel Institute of Technology, Haifa 32000, Israel*

[b] *Department of Chemical Engineering, Technion — Israel Institute of Technology, Haifa 32000, Israel*

Received 31 October 2000; received in revised form 22 January 2001; accepted 19 February 2001

Abstract

The synthesis and characterization of Th-MCM-41 and U-MCM-41 new members of a growing family of hexagonal packed metallo-silicates molecular sieves are described. The synthesis of these materials was achieved by a "liquid crystal templating" mechanism (LCT), with a C_{16} length chain for the cationic amine surfactant, when the additional metal salt was added to the synthesis mixture, forming large agglomerates imbedded within the silica matrix. For uranium, the synthesis was performed using $UO_2(NO_3)_2{\cdot}6H_2O$ as a precursor whereas for the thorium, the reaction was carried out using $Th(NO_3)_4{\cdot}5H_2O$ (thorium nitrate pentahydrate) as the metal source. The incorporation of the uranium into the mesoporous material was performed via a complementary basic synthesis, whereas for the latter thorium, an acidic route was utilized.

The Th-MCM-41 and U-MCM-41 were characterized by small angle X-ray scattering (SAXS), specific surface areas (Brunauer–Emmett–Teller (BET)), scanning electron microscopy (SEM) equipped with an energy dispersive spectrometer and X-ray photon spectroscopy (XPS). SAXS study revealed the mass fractal scattering characteristics of these materials with fractal dimension in the range of 2.78–2.95 Å. These materials also exhibited a hexagonal array of cylindrical mesopores from 27 to 30 Å in size, surface areas of over 850 m^2/g, and high thermal and hydrothermal stability. The incorporation of actinide metals into the MCM-41 matrixes was 3.23 (2) at.% of Th and 11.22 at.% for U, respectively. SEM study revealed the particle morphologies with large monolithic aggregates whereas XPS indicates the geometric configuration and coordination of the metal in the silicate. We have found that in U-MCM-41, most of the uranium metal in encounter in an octahedral geometry arrangement whereas in the Th-MCM-41, the corresponding thorium metal is assemble in tetrahedral environment In addition, the catalytic reactivity of these materials was measured for the hydroxylation of phenol and the alkylation of 2,4-di-tert-butylphenol with cinnamyl alcohol. © 2001 Published by Elsevier Science B.V.

Keywords: Th-MCM-41; U-MCM-41; Liquid crystal templating; Catalysis; Mesoporous materials; Hydroxylation; Alkylation

1. Introduction

A new family of mesoporous molecular sieve materials, MCM-41, was discovered in 1992 by researches at the Mobil Corporation [1,2]. The MCM-41 mesoporous material consists of uniform hexagonal arrays

* Corresponding author. Tel.: +972-4-8292680; fax: +972-4-8233735.
E-mail address: chmoris@techunix.technion.ac.il (M.S. Eisen).

1381-1169/01/$ – see front matter © 2001 Published by Elsevier Science B.V.
PII: S1381-1169(01)00109-1

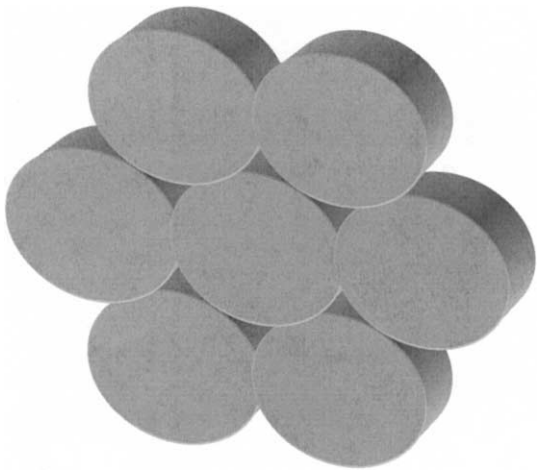

Fig. 1. MCM-41 after calcination showing the honeycomb structure of the silica matrix.

of linear channels that are constructed with a silica matrix like a honeycomb (Fig. 1).

By the use of different surfactant chain lengths, in which the silicates polymerize hydrothermally forming the honeycomb matrix structure, the properties of these mesoporous materials can be tailored [3]. The surfactant is easily removed by calcination at 750–800 K leaving silica honeycombs mesoporous materials with pore diameters in the range of 1.6–10 nm. The large pore size in the mesoporous MCM-41, as compared with the pore size in conventional zeolites (<1.4 nm) has opened a large number of applications. These materials attract much attention as new catalytic materials and host for large molecules [4,5].

The original preparation of hexagonal mesoporous silica MCM-41 was achieved through a S^+I^- electrostatic micellar assembly mechanism. The mechanism consists of the reaction of a quaternary ammonium cations (S^+), which plays the role of surfactant as well as a structure-directing agent, and the oligomeric silicate anions (I^-) [4].

MCM-41 is based on silica frameworks lacking of acid sites and ion exchange capacity, these properties limit its application in catalysis and adsorbents. To overcome the limitations, metals, such as electrophilic aluminum, has been incorporated within the framework of the MCM-41 although, in some cases dealumination occurs upon calcination [5]. Recently, Al-MCM-41 has been shown to have excellent ion exchange capacities and high hydrothermal properties [5].

Several attempts have been made to prepare MCM-41 with various amounts of Al or other metals, which can endow silicates with desirable properties. Thus, the substitution of framework silicon by other tetravalent or trivalent metal such as Ti, [6–13] V, [7,14–17] Cr, [7] Mo, [7] Sn, [18,19] Mn, [7,20] has led to modified silica structures containing various amounts of these ions.

The importance of the textural mesoporosity in increasing the catalytic activity has been reported for many processes. For example, higher conversion for peroxide oxidation of miscellaneous substrates have been reported for Ti-, V-, Cr-HMS (HMS is hexagonal molecular sieves) materials as compared to the resembling MCM-41 substituted material [6–17]. In addition, Ti-MCM-41 has been reported to exhibit a higher catalytic activity in the epoxidation of α-pinene, [21] in the oxidation of benzene [22] and in the oxidation of aniline [23] as compared to the analogous Ti-HMS materials. Therefore, it seems that the discrepancies in evaluating the relative catalytic activities of HMS and MCM-41 metal based materials is still obscure and may be linked to the textural porosity but also to the sensitivity to the reaction parameters such as solvent polarity, temperature, etc.

A conceptual question rises regarding the real electrophilicity of the metal atoms in metal-MCM-41 materials. It seems that the higher the electrophilic character of the metal the better their performance in specific catalytic organic transformations. Moreover higher the coordinative unsaturation the higher the reactivity expected. Thus, it is plausible to expect that lanthanide or even actinide-based mesoporous materials will exhibit unique reactivities.

In this work we present for the first time the synthesis and characterization of very electrophilic actinide metals, thorium and uranium as components of MCM-41 materials. The characterization was made by small angle X-ray scattering (SAXS), specific surface areas (Brunauer–Emmett–Teller (BET) method), scanning electron microscopy (SEM) and X-ray photon spectroscopy (XPS). In addition the catalytic activities of the mesoporous materials in the hydroxylation of phenol and in the alkylation of

2,4-di-tert-buthylphenol with cinnamyl alcohol are reported.

2. Experimental section

2.1. Chemicals

The sources of silica were sodium silicate (14% NaOH, 27% SiO_2, $d = 1.39$ g/ml) and tetraethyl orthosilicate (TEOS) obtained from Aldrich and used as received. The surfactants utilized were the quaternary ammonium salt with the formula $C_{16}H_{33}N(CH_3)_3Cl$ (cetyl trimethyl ammonium chloride = CTAC; 25% aqueous solution, $d = 0.968$ g/ml) and formula $C_{16}H_{33}N(CH_3)_3Br$ (cetyl trimethyl ammonium bromide = CTAB), obtained from Aldrich and used as received. The thorium salt used was $Th(NO_3)_4{\cdot}5H_2O$ (thorium nitrate pentahydrate) obtained from MERK. The source of uranium salt was $UO_2(NO_3)_2{\cdot}6H_2O$ (uranyl nitrate hexahydrate) obtained from Fisher. Phenol was purchased from BDH; hydrogen peroxide (30%) was purchased from Fisher; 2,4-di-tert-butylphenol and cinnamyl alcohol were purchased from Aldrich. The organic compounds were used without additional treatments. MCM-41 was prepared as described in [20].

3. Preparation of materials

3.1. Synthesis of Th-MCM-41

The synthetic route used for the preparation of Th-MCM-41 follows the incorporation of the metal as thorium nitrate pentahydrate in acidic water solution to avoid precipitation of salt and then by bringing the solution to a basic pH.

To a 10 ml of aqueous solution containing 2.0 g (5.5 mmol) of CTAB was added 2.2 ml of a solution of sodium silicate with an additional 4 ml of water. The reaction was stirred for 30 min and 1 ml of 1N HCl is added to bring the solution to pH = 2.5. Then 0.014 g (2.45 mmol) of $Th(NO_3)_4{\cdot}5H_2O$ was added and the reaction mixture was stirred for an additional 30 min. To the reaction mixture, 2 ml of NH_4OH are added to bring the solution to pH = 11 and the reaction is stirred for 30 min. The reaction mixture is introduced into an autoclave and heated to 100°C for 56 h.

The solid precipitate was recovered by filtration, and washed several times with distilled water, and dried in air at ambient temperature for 24 h. The template removal was achieved by calcination in air at 550°C for 4 h, using a ramping rate of 20°C/min.

The molar composition of the as-synthesis gel was

$$2.46\,SiO_2 : 1\,CTAB : 0.97\,Na_2O : 0.18\,HCl : 5.39\,NH_3 : 181.80\,H_2O : 0.044\,ThO_2$$

3.2. Synthesis of U-MCM-41

To a 10 ml of aqueous solution containing 0.73 g (0.55 mmol) of CTAC (25% aq. solution) was added 1.3 ml (2.6 mmol) of a 2N NaOH solution and the mixture was stirred for 40 min. To this solution 0.058 g (0.115 mmol) of $UO_2(NO_3)_2{\cdot}6H_2O$ powder was added and stirred for an additional 30 min. To the stirring mixture, 1.02 ml (4.6 mmol) of the precursor TEOS was added under vigorous stirring conditions and the reaction mixture was stirred for 48 h at ambient temperature in a sealed flask. The basicity of the reaction was all the time maintained at pH = 11 by adding the corresponding amounts of a 2N NaOH solution.

The solid precipitate was recovered by filtration, and washed several times with distilled water, and dried in air at ambient temperature for 48 h. The template removal was achieved by calcination in air at 550°C for 4 h, using a ramping rate of 2°C/min.

The molar composition of the as-synthesis gel was

$$1\,TEOS : 0.12\,CTAC : 0.56\,NaOH : 124\,H_2O : 0.025\,UO_2$$

4. Analytical techniques

The data of SAXS were obtained using slit-collimated Kratky camera (A. Par Co), Ni-filtered Cu Kα radiation, 20 kV on the tube, one-dimensional detector. Samples of approximately 1 mm thick were prepared by sprinkling the powdered samples on adhesive cellophane tape used as windows with 2.0 cm × 0.5 cm inner size. Data was collected in the interval $0.01 < \boldsymbol{h} < 0.64\,\text{Å}^{-1}$ ($0.1 < \boldsymbol{h} < 6.4\,\text{nm}^{-1}$) to determine the surface and mass fractal dimension of the small particle materials The wave vector $\boldsymbol{h}$ is defined as, $\boldsymbol{h} = (4\pi/\lambda \sin(2\theta/2)$, where $\lambda = 1.54$ is

the wave length and 2θ is the scattering angle. Scattering data were corrected for slit-smearing before sample structure parameter calculations. Two to three samples of the same type were examined to evaluate the standard deviation.

Shifts in the position of the first correlation peak for MCM-41, Th-MCM-41 and U-MCM-41 samples were taken as being indicative of changes in the average pore–pore separation. The light areas in the images correspond to a lack of scattering matter (pores), and the dark areas are concentration of scattering materials (walls).

Theoretically, the SAXS scattering supplies a direct measure of the fractal nature of an object [24] over a large in length scale, $1/\boldsymbol{h}$. This inverse relationship indicates that small characteristic sizes are observed at large h values and vice versa. For example, the framework pores will give rise to the small angle scattering intensity whereas the porous particles themselves are the large features contributing to the scattering.

Fractal objects are known to produce a power law scattering following the rule $I(\boldsymbol{h}) = \boldsymbol{C}\boldsymbol{h}^{P}$ (C = constant and P = a power number) [25]. When the SAXS data is plotted as a log of the intensity versus a log scale of the $\boldsymbol{h}$ value, straight line-segments are obtained. The matters that scatter with P values equal -4 (Porod scattering) are known to have a non-fractal surface morphology. When the power laws are between $-4 \leq P \leq -3$, surface fractal structures are observed with a surface fractal dimension of $D_s = 6 + P$. The surface area corresponding to this P value is approximately $A \sim r^{D_s}$,, (r = size of particle). Power laws in which $-3 \leq P \leq -1$ are indicatory of mass fractal structure where the mass fractal dimension $D_m = -P$. Mass fractal are porous aggregates of primary particles for which the mass scales as $M \sim r^{D_m}$ [26,27].

SEM was performed on a JEOL JSM5400 scanning electron microscope using conventional sample preparation and imaging techniques. The SEM microscope is equipped with an energy dispersive spectrometer (Voyager, Noran Instr.) which was used for obtaining element and atomic weight compositions of the samples. The XPS (SPECS Instr.) measurements were performed using a spherical analyzer and an Al Kα (1486.6 eV) anode.

The BET surface areas (m^2/g) measurements were calculated from the linear part of the BET according to the IUPAC recommendations [28]. The measurements were carried out with N_2 adsorption–desorption procedure using a volumetric gas adsorption Flowsorb II 2300 equipment.

NMR spectra were recorded on Bruker AM 200 and AM 400 spectrometers. Two-dimensional spectroscopic techniques as DEPT, JMOD, COSY, C–H correlation and HeteroCOSY were used to assign the signals to each of the carbons of the products. Chemical shifts for ^{1}H NMR and ^{13}C NMR were referenced to internal solvent resonances and are reported relative to tetramethylsilane. GC–MS experiments were conducted in a GC–MS (Finnigan Magnum) spectrometer. Gas chromatography (GC) experiments were conducted on a Varian 3800 instrument with a capillary column 30 m, 0.25 mm i.d. DB-5 (purchased at J & W Scientific). ICP experiments were performed with a Thermo Jarrel Ash Atom Scan 25 spectrometer.

5. Catalytic reaction

5.1. Hydroxylation of phenol with hydrogen peroxide to catechol and hydroquinone

An amount of 0.2 g of the corresponding catalyst was mixed with 45 ml of deionized water, 2 g (21.0 mmol) of phenol and 2 g (18.0 mmol) of hydrogen peroxide (30%) in a 100 ml round-bottom flask fitted with a water cooled condenser and a magnetic stirrer. The reaction mixture was heated to 80°C and maintained at this temperature for 15 h. The reaction products were filtered to remove the catalyst and the water was removed by an azeotropic distillation with benzene using a Dean–Stark column. Excess of the benzene was removed by means of an evaporator. The reaction products were analyzed by GC and NMR spectrometry and compared to clean samples. The extraction of the organic products is necessary to remove the water that damage the GC columns and exhibit a large signal in the NMR spectrometer.

5.2. Alkylation of 2 4-di-tert-butylphenol with cinnamyl alcohol

In a 100 ml flask equipped with a water condenser containing 0.134 g (1 mmol) of cinnamyl alcohol and 0.206 g (1 mmol) of 2,4-di-tert-butylphenol were

added to 50.0 ml of isooctane used as the solvent. The reaction mixture was heated to 90°C. When the temperature equilibration was achieved the required amount of the catalysts was introduced through a solid addition funnel and the reaction was heated for an additional 24 h. The catalyst was filtered and extracted with dichloromethane to recover adsorbed reaction products. The solution from the reaction and the catalyst extraction were combined and distilled to remove the solvent. The product flavan was analyzed by GC, GC–MS and NMR spectrometry and by its comparison to known samples, whereas the isomeric benzofuran was analyzed by GC–MS.

6. Results and discussion

The mesoporous-structured MCM-41 metal-based materials were prepared following the electrostatic mechanism route (S^+I^-) under different conditions. For the uranium salt a basic procedure was followed to introduce the metal into the matrix, whereas for the thorium salt an acidic route was utilized.

For uranium, the reaction of the quaternary cetyl trimethyl ammonium chloride (S^+) with NaOH, in water, forms and array of micellar tubes. $UO_2(NO_3)_2{\cdot}6H_2O$, is added as the source of uranium and TEOS, the inorganic silicate, is added to form the silica matrix. These inorganic silicates, which are present in the reaction mixture, are expected to produce the inorganic structures, reflecting the hexagonal micellar array. For uranium, the slightly soluble oligomeric octahedral $UO_2(OH)_2$ that will be formed upon the addition of $UO_2(NO_3)_2{\cdot}6H_2O$ to the soda caustic solution, plausible react with the TEOS replacing some of the silica atoms sites in the inorganic hexagonal structure around the micelles (see below Fig. 2). In the preparation of the corresponding Th-MCM-41 mesoporous material an acidic procedure was followed. The objective to pursue such a procedure is to avoid the precipitation of ThO_2 in basic solutions. Hence, we decided to introduce the metal salt in an acidic solution and slowly bringing the pH of the solution to the basic regime (pH = 11), in which the inorganic silicates form the hexagonal matrix [5]. It is important to point out that the first step in the synthesis, the reaction of CTAB with a base is a crucial step in the micellar formations and cannot

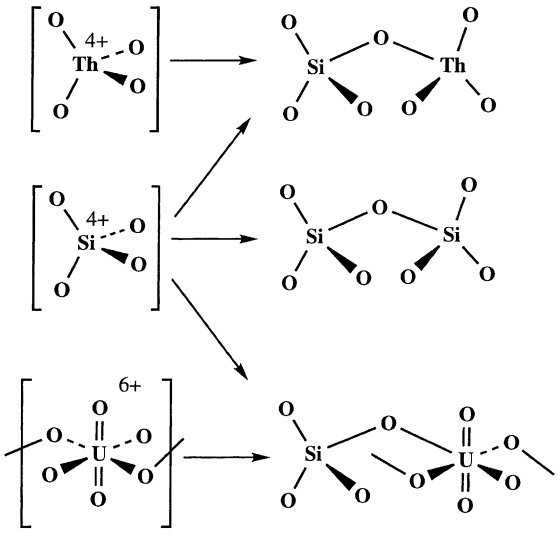

Fig. 2. Proposed building blocks for the formation of metal substituted hexagonal silica honeycomb frameworks.

be omitted. CTAB will react with the base forming a mixture of ammonium hydroxide/ammonium bromide polar heads, which will ensure the micellar formation. The silicate added ensures the formation of the inorganic matrix around the micelles and will keep their configuration even after the addition of a mineral acid [20]. For both thorium arid uranium, the as-synthesized products were easily isolated from the synthesis mixtures by filtration and water rinsing. The final products were obtained by calcination in air, for water and surfactant removing.

Thus, its seems that at least two types of bonding for the metal can be expected in the MCM-41 materials. The first type of bonding is between metal atoms bridged by oxygen atoms (U–O–U, Th–O–Th) whereas the second type is bonding between uranium and silicon atoms of the silicates also bridged by oxygen atoms (U–O–Si, Th–O–Si) as described in Fig. 2. To gather some information regarding the bonding and the geometrical environment of the metals in the MCM-41 mesoporous materials, XPS experiments have been investigated.

XPS experiments on the corresponding mesoporours Th-MCM-41 arid U-MCM-41 exhibits unique binding energy for the $4f_{5/2}$ and $4f_{7/2}$ signals. For the earlier the $4f_{7/2}$ signal appear at 330.3 eV with $D = 9.34$ eV which appear at slightly lower energy

as compared to ThO_2 (334.5 eV) and is similar to the literature value for Th–O–Si signals in glasses [29]. For the latter mesoporous material the $4f_{7/2}$ XPS signal appear at 379.5 eV with $D = 10.86$ eV which is in agreement for an octahedral U (+6) compound embedded in glasses with U–O–Si bonds and ruling out U (+4) compositions [30,31]. Important to point out that it is still possible that some of the bonding in both mesoporous materials contain M–O–M bonds although, it seems that they are not the major components.

7. Characterization of MCM samples

SAXS studies has been used to characterize fractal dimensions, particle sizes and other structural parameters of porous silicas and micelles confined in porous silica [25,32,33] SAXS studies have been reported for mesoporous silica materials prepared with surfactants [34–38] and recently, SAXS has been used to describe the unique mass fractal character of surfactant-templated silica aerogels (STSA) with a hexagonal MCM-41 framework structure [39]. In this work we have studied the small angle scattering characteristics of hexagonal mesostructures silicas formed through the general electrostatic assembly route, in particular, MCM-41 (for comparison), and Th-MCM-41 and U-MCM-41 over the $\boldsymbol{h}$ range, $0.01 < \boldsymbol{h} < 0.64^{-1}$. Plots of the SAXS data, along with the corresponding least-square fit to the power law, are plotted in Fig. 3.

Power law scattering is seen in the low $\boldsymbol{h}$ region although, no surface to mass fractal scattering transition is observed. A least-squares fit to the power-law scattering at mid $\boldsymbol{h}$ values yield an exponent of −2.95 (0.02) for MCM-41, −2.78 (0.02) for Th-MCM-41 and −2.94 (0.02) for U-MCM-41 where the numbers in parenthesis are the standard deviation of the last figure (Fig. 4). All three types of samples (MCM-41 and MCM-41 with thorium and uranium) show a similar slope of $P = -2.78$ to −2.95, which is attributed to mass fractal scattering with fractal dimension $D_m = -P$ (Fig. 4) [26]. This number indicates that the mass scale is $M \sim r^3$, [27] with normal continuous mass distribution surface fractal moieties.

The multiple correlation peaks which are evident in the scattering curves of MCM-41, Th-MCM-41 and U-MCM-41 (Figs. 3 and 4) indicate that the mass unit with pores are well ordered. All the curves are consistent with the hexagonal array of framework pores. MCM-41 is the best ordered [40] structure with four correlation peaks as already observed at $d_{100} = 3.83$ nm. The correlation peaks for MCM-41, Th-MCM-41 and U-MCM-41 are giving in Fig. 5 and the corresponding d values are summarized in Table 1. Interestingly, there is a slightly change in the a dimension when comparing MCM-41 with the

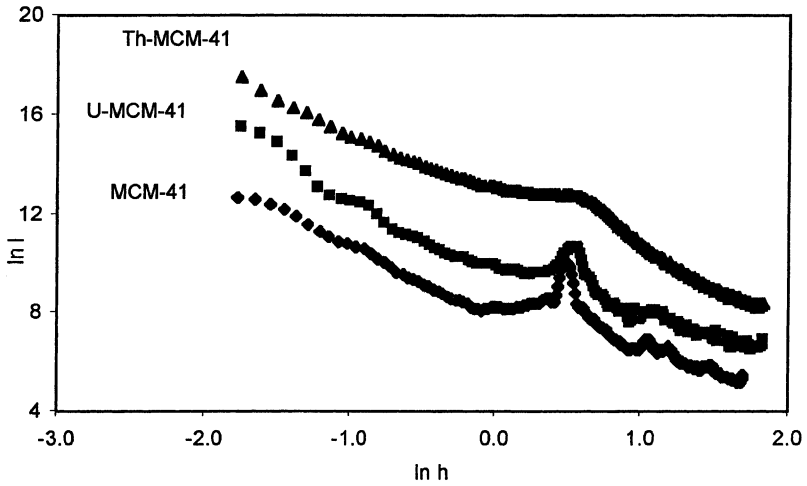

Fig. 3. Porod plot of $\ln I$ (intensity) vs. $\ln \boldsymbol{h}$ ($\boldsymbol{h} = \text{nm}^{-1}$) for plain and metal substituted MCM-41 calcinated samples.

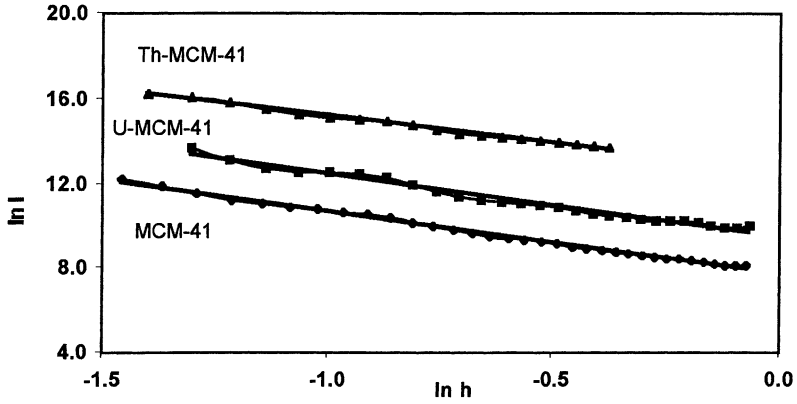

Fig. 4. Line approximation of Porod plot of $\ln I$ (intensity) vs. $\ln \boldsymbol{h}$ ($\boldsymbol{h} = \mathrm{nm}^{-1}$).

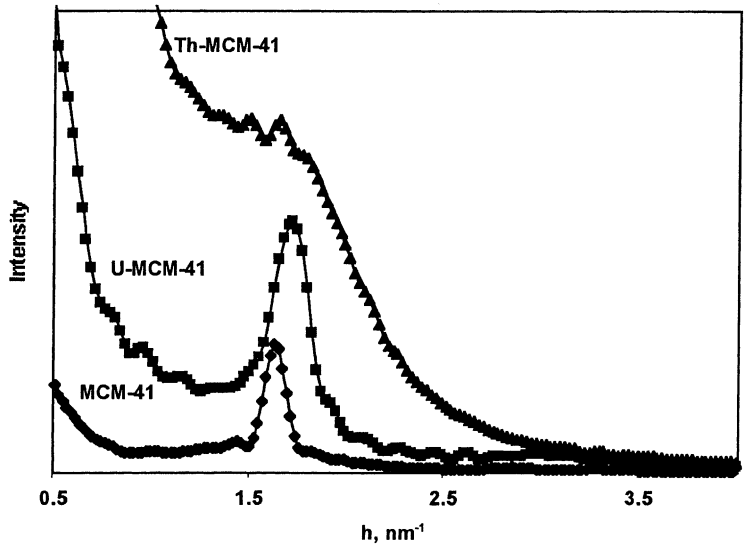

Fig. 5. Diffraction of calcinated plain and metal substituted MCM-41 samples.

Table 1
Lattice parameters for MCM-41 samples, d (1 0 0) plane distance, and a-unit center to center distance

Sample	d (1 0 0) (Å)	d (1 1 0) (Å)	d (2 0 0) (Å)	d (2 1 0) (Å)	a (Å)
MCM-41	38.315	22.125	19.155	14.48	44.24
U-MCM-41	36.745	21.09	18.27	13.81	42.43
Th-MCM-41	38.485	–	–	–	44.44

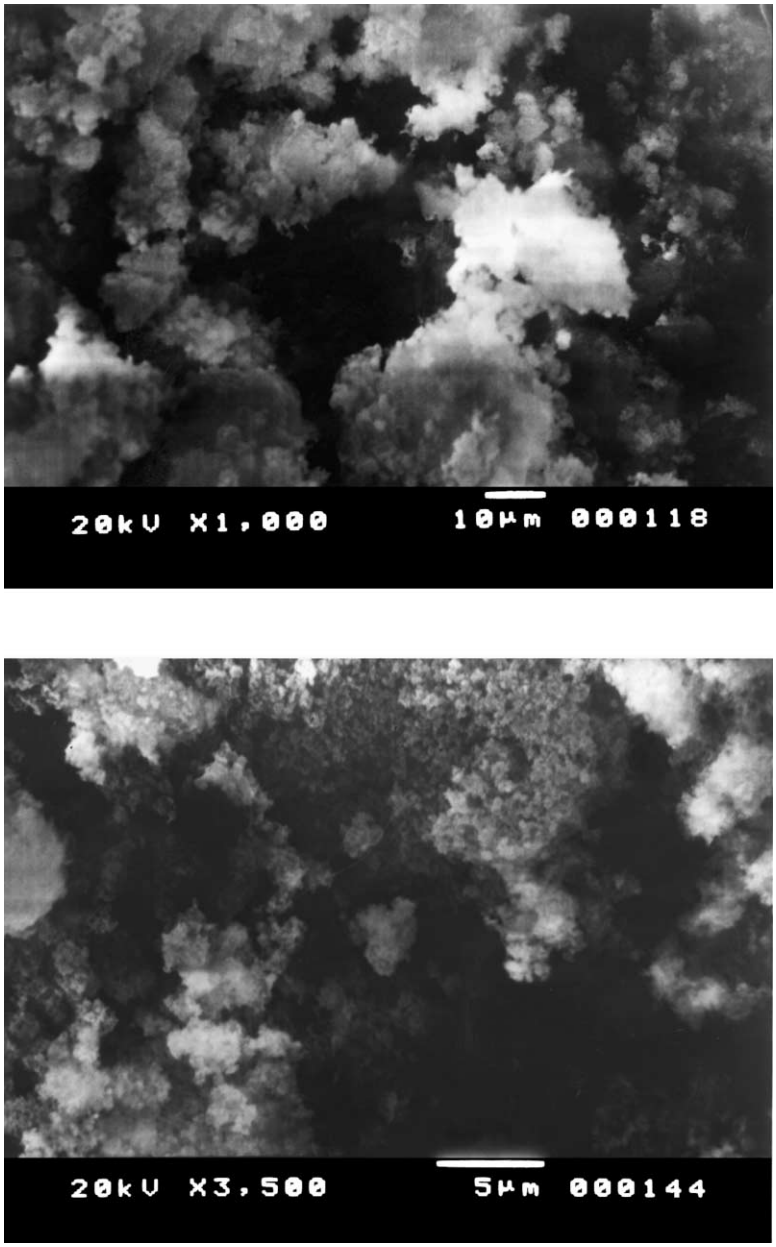

Fig. 6. SEM pictures of TH-MCM-41 (top) and U-MCM-41 (bottom).

metal substituted MCM-41 as already observed for some tin derivatives [19].

It is important to point out that for each mesoporous material a standard deviation of 0.2 for the D_m value was obtained when an average of a large number of examined samples were plotted together arguing for a high reproducibility of the reactions. For MCM-41 and U-MCM-41 XRD measurements shows the 1 0 0, 1 1 0, 2 0 0, and 2 1 0 reflections. For the Th-MCM-41 only the 1 0 0 reflection is observed. The absence of

Table 2
Average size of crystals formed by cylindrical units into MCM-41 samples

Sample	L (Å)
MCM-41	486
Th-MCM-41	136
U-MCM-41	312

higher angle diffraction peaks is attributed to excessive broadening of the $hk0$ reflections, due to too small scattering domain sizes as observed in Table 2 [41].

The average size of the crystals formed on the cylinder units can be obtained using Scherrer's equation.

$$L = \frac{0.9\lambda}{\beta \cos\theta}$$

where λ is wavelength of the X-rays, 2θ the diffraction angle, β the the pure X-ray diffraction breadth, L the crystal size perpendicular to the cylinders axis in both dimensions (x, y). The results are presented in the Table 2.

The BET surface area of the hexagonal silicate materials were measured by nitrogen adsorbtion–desorbtion yielding the following values: MCM-41 = 770 m^2/g, Th-MCM-41 = 866 m^2/g and U-MCM-41 = 897 m^2/g. The three values are slightly different although, as expected. The metal substituted MCM-41 have a larger surface area as compared to the plain MCM-41 with tetrahedral thorium replacing the tetrahedral silicon in the matrix. In addition a slightly large a value is obtained for the Th-MCM-41 as compared to the corresponding MCM-41. For uranium the situation is different, since now an octahedral metal is replacing a tetrahedral position, causing a larger surface area due to the coordinative holes and a slightly contraction in the unit cell a value.

The pore size of the Th-MCM-41 and U-MCM-41 can be calculated from the a value and the wall thickness for MCM-41. Thus, for Th-MCM-41 and U-MCM-41 the pore size can be calculated to be in the range of 27–30 Å [3]. The percent of metal incorporation within the silica framework was obtained from the SEM which is equipped with an energy dispersive spectrometer. The calcinated samples were measured and the values for the incorporation of the actinides into the silica matrix were 3.23 (2) at.% of Th and 11.22 at.% of U, for Th-MCM-41 and U-MCM-41, respectively.

Scanning electron micrographs for the corresponding Th-MCM-41 and U-MCM-41 (Fig. 6), exhibit similar particle morphologies with large monolithic aggregates, in contrast to the non-uniform aggregates of small particles obtained in HMS materials [42].

8. Catalysis studies

Some metal containing MCM-41 materials have been found to be active catalysts for a number of organic chemistry transformations [6,7–20]. We have probed the actinide-MCM-41 materials in two catalytic processes. The first is the hydroxylation of phenol in water, the second reaction is the alkylation of a substituted phenol with an alcohol to obtain flavan. This reactions were studied to compare the real Lewis acidity of the actinides into the mesoporous matrix and to compare to other Lewis acid metal-MCM-41 materials.

8.1. Hydroxylation of phenol

The catalytic activity of the actinide-MCM-41 compounds was studied for the hydroxylation of phenol (Eq. (1)) and the results are summarized in Table 3.

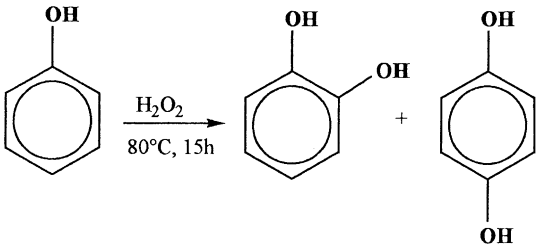

(1)

As can be seen in Table 3, Th-MCM-41 was found to be the most active catalysts whereas the corresponding U-MCM-41 shows no activity at all. The lack of activity for the corresponding U-MCM-41 can be rationalized due to the higher oxidation state and acidity of U (+6) as compared to Th (+4). It seems plausible that the high acidic uranium metal is unavailable to donate on oxygen atom to the phenol molecule in his high oxidation state not favoring the hydroxylation pathway. Interestingly, the leaching of the thorium

Table 3
Hydroxylation of phenol by various heterogeneous metal containing supports under similar conditions[a]

Catalyst[a]	Conversion (%)	Selectivity	
		CT[b] (%)	HQ[c] (%)
FeAPO-11 [43]	262[d]	51.1	48.9
$AlPO_4$-11 [43]	11.5[d]	44.1	55.8
SAPO-11 [43]	7.2[d]	52.2	47.8
MgAPO-11 [43]	7.3[d]	75.8	24.2
CoAPO-11 [43]	23.1[e]	55.4	44.6
Fe-MnAPO-11 [43]	18.0[e]	52.8	47.2
TS-1 [43]	29.0[e]	31.3	68.7
Th-MCM-41	67.2[d]	48.8	51.2
U-MCM-41	0.0	–	–

[a] An amount of 0.2 g catalyst; 2 g of phenol; 2 g of 30% H_2O_2; 45 ml of water at 80°C.
[b] CT: catechol.
[c] HQ: hydroquinone.
[d] Reaction time: 15 h.
[e] Reaction time: 5 h.

metal (measured by ICP) in the water solution after the reaction is below the limit of detection (<5 ppb), whereas the amount of leaching of uranium is less than 2% from its initial content, indicating that the Th-MCM-41 has a better thermal stability as compared to U-MCM-41. The larger activity of the thorium compound over other structures can be rationalized due to the high surface area of Th-MCM-41 as compound to the aluminophosphate compounds or the pure titanium silicate TS-1. Recently, it has been reported that Ti-MCM-41 is able to hydroxylate phenol only to hydroquinone although, the obtained catechol was found to follow polymerization [42]. The selectivity of the Th-MCM-41 as compared to other systems is quite similar (besides MgAPO-11) indicating that no difference in adsorption rates are observed for the *o*- and *p*-isomers as found for Ti-MCM-41.

8.2. Alkylation of 2,4-di-tert-butylphenol with cinnamyl alcohol

Highly acidic Al-MCM-41 has been recently reported as an effective catalyst for the Friedel Crafts alkylation reaction involving the substrate 2,4-di-tert-butylphenol with cinnamyl alcohol to yield flavan (**1**) and in some cases with the concomitant formation of 4-tert-butyl phenol (**2**) and the corresponding substituted benzopyran (**3**) (Eq. (2)) [43].

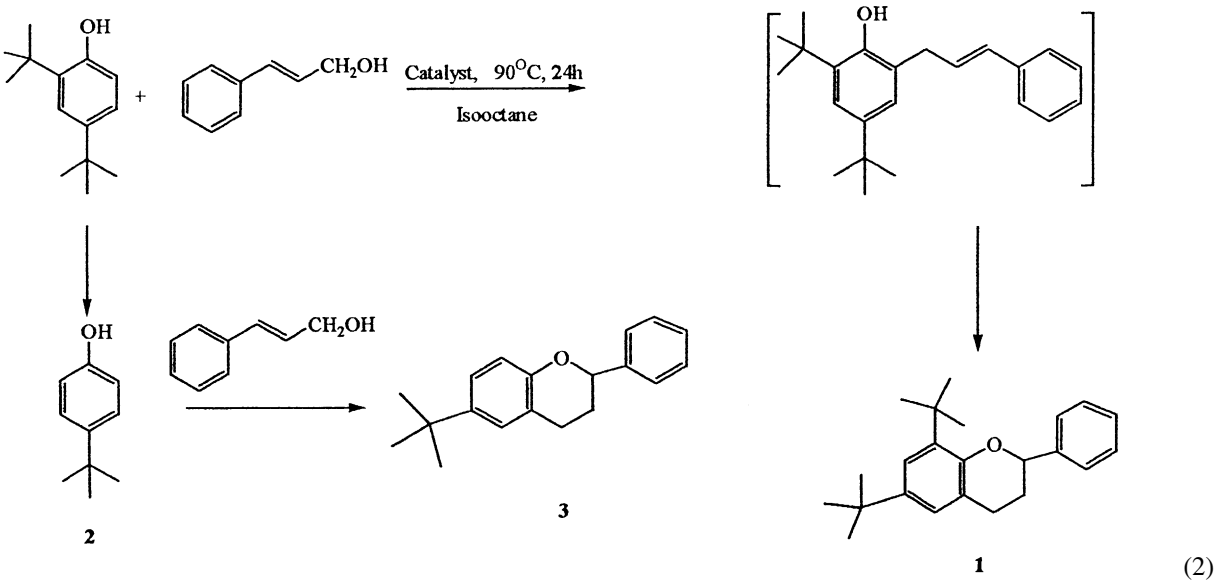

(2)

The formation of flavan is consisted of two consecutive steps. The Friedel Crafts alkylation giving the intermediate cinnamyl phenol followed by an intramolecular ring closure to give the final flavan product **1**. Hence, we have chosen this probe reaction to study the acidic catalytic properties of the newly

Table 4
Alkylation of 2,4-di-tert-butylphenol (DTBP) with cinnamyl alcohol

Catalyst	Conversion of DTBP[a,b] (%)	Flavan yield (%)	Selectivity (%)	
			1	4
Al-MCM-41	47.2	33.9	71.8	NA[c]
U-MCM-41	15.5	8.9	34.1	65.9
Th-MCM-41	7.1	5.0	70.5	29.5
Si/Al	44.0	6.0	13.1	NA

[a] An amount of 0.134 g cinnamyl alcohol; 0.206 g 2,4-di-tert-butylphenol; 50 ml isooctane; reaction temperature: 90°C; reaction time: 24 h.
[b] Cinnamyl alcohol conversion is 100% in every reaction.
[c] NA: not available; Si/Al: amorphous silica–alumina (25%) [43].

prepared actinide-MCM-41 mesoporous materials and its corroboration with the above presented results.

The reaction is carried out with an equimolar solution of 2,4-di-tert-butylphenol and cinnamyl alcohol in isooctane, which was heated at 90°C in the presence of the corresponding catalyst for 24 h. The

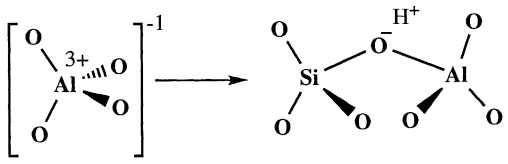

Fig. 7. Formation of acidic sites when aluminum is included into a silica matrix.

catalytic properties of Th-MCM-41 and U-MCM-41 along with those reported with Al-MCM-41 are presented in Table 4. The conversion values for 2,4-di-tert-butylphenol to flavan using Th-MCM-41 and U-MCM-41 are low as compare to Al-MCM-41 or to plain amorphous silica–alumina (25%) (Si/Al in Table 4). This result is rationalized by the larger acidic properties of the Al-MCM-41 as compared to the actinide-MCM materials. The actinides, which are isolobal to the metals of the Groups 4 and 14 of the periodic table and isolobal to silicon, upon their incorporation into the matrix, will maintained an electronic close shell configuration (Fig. 2).

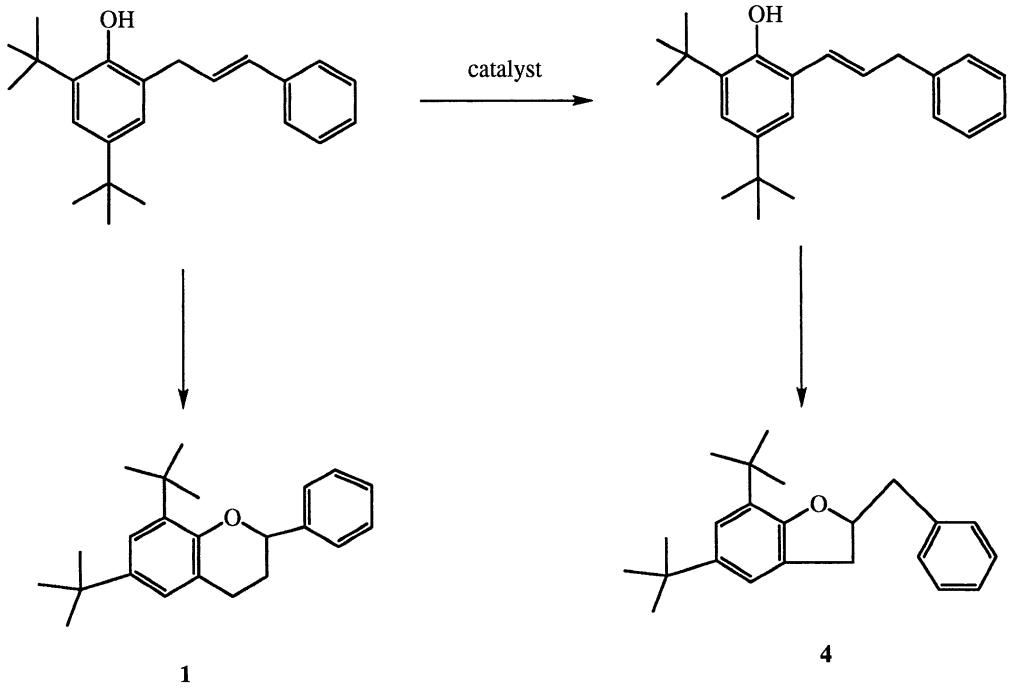

Fig. 8. Intermolecular cyclization of cinnamyl phenol intermediate to the products **1** and **4**.

When a metal from Groups 3 or 13 is incorporated into the tetrahedral array of the silica, a highly active acidic position remains free for catalysis (Fig. 7).

Thus, a lower reactivity is indeed expected for the actinides-MCM materials in the Friedel Crafts reaction as compared to Al-MCM-41. When comparing the selectivities of the actinides it is notable to point out that Th-MCM-41 and U-MCM-41 produce only two products **1** and **4** with no formation of compounds **2** or **3** as obtained for Al-MCM-41. Compound **4** is obtained by an isomerization of the double bond process before the ring closure is completed forming a five membered ring (Fig. 8).

Interestingly the selectivity of the actinides towards compounds **1** and **4** are opposite indicating the different reactivities of the two metals due to their difference in oxidation states.

Although, U-MCM-41 is more acidic and active than Th-MCM-41 for the alkylation reaction, the Th-MCM-41 is more selective allowing a better discrimination between the selectivities of compounds **1** and **4**.

Besides flavan or the benzofuran compounds, different products arising from the oligomerization and polymerization of cinnamyl alcohols were obtained, although, due to their large number, the fully characterization is in progress and will be reported in a different paper.

9. Conclusions

Actinide-based MCM-41 materials have been prepared by an electrostatic micellar assembly mechanism using acidic and basic routes for Th and U metals, respectively. SASX study on the new materials shows only a mass fractal scattering with fractal dimension of 2.78 (0.02) for Th-MCM-41 and 2.94 (0.02) for U-MCM-41. Th-MCM-41 has been shown to be a most active catalyst for the hydroxylation of phenol with high conversions and almost equimolar yields to catechol and hydroquinone whereas U-MCM-41 did not show any catalytic activity on the hydroxylation of phenol. In addition, Th-MCM-41 and U-MCM-41 were found to be active for the Friedel Crafts alkylation of 2,4-di-tert-butyiphenol with cinnamyl alcohol towards flavan and its isomeric benzofuran.

Acknowledgements

This research was supported by the Ministry of Science, Government of Israel, by the Henri Gutwirth Fund for the Promotion of Research, by the Fund for the Promotion of Research at the Technion, by the Technion Water Research Institute for Instrumentation Grant and by the Technion V.P.R. fund. B.R. and R.T. thank the Ministry of Science for post-doctoral fellowships.

References

[1] C.T. Kresge, M.E. Leonowicz, M.E. Leonowicz, W.J. Roth, J.C. Vartuli, J.S. Beck, Nature 359 (1992) 710.
[2] J.S. Beck, J.C. Vartuli, W.J. Roth, M.E. Leonowicz, C.T. Kresge, K.D. Schmitt, C.T.-W. Chu, D.H. Olson, E.W. Sheppard, S.B. McCullen, J.B. Higgins, J.L. Schlenker, J. Am. Chem. Soc. 114 (1992) 10834.
[3] P.T. Tanev, T.J. Pinnavaia, Chem. Mater. 8 (1996) 2068.
[4] R. Ryoo, J.M. Kim, J. Chem. Soc., Chem. Commun. (1995) 711.
[5] J.M. Kim, J.H. Kwak, S. Jun, R. Ryoo, J. Phys. Chem. 99 (1995) 16742–16747.
[6] S.A. Bagshaw, E. Prouzet, T.J. Pinnavaia, Science 269 (1995) 1242.
[7] W. Zhang, J. Wang, P.T. Tanev, T.J. Pinnavaia, J. Chem. Soc., Chem. Commun. (1996) 253.
[8] W. Zhang, J. Wang, P.T. Tanev, T.J. Pinnavaia, J. Chem. Soc., Chem. Commun. (1996) 979.
[9] P.T. Tanev, M. Chibwe, T.J. Pinnavaia, Nature 368 (1994) 321.
[10] W. Zhang, M. Fröba, J. Wang, P.T. Tanev, T. Pinnavaia, J. Am. Chem. Soc. 118 (1996) 9164.
[11] A. Croma, M.T. Navarro, J. Perez-Pariente, J. Chem. Soc., Chem. Commun. (1994) 147.
[12] A. Croma, M.T. Navarro, J. Perez-Pariente, Stud. Surf. Sci. Catal. 84 (1994) 69.
[13] O. Franke, J. Rathousky, G. Schulz-Ekloff, I. Starek, Z. Zukal, Stud. Surf. Sci. Catal. 84 (1994) 77.
[14] K.M. Reddy, I. Moudrakovski, A. Sayari, J. Chem. Soc., Chem. Commun. (1994) 1059.
[15] J.S. Reddy, A. Sayari, J. Chem. Soc., Chem. Commun. (1995) 2231.
[16] J.S. Reddy, P. Liu, A. Sayari, Appl. Catal. A 7 (1996) 148.
[17] A. Chenite, Y. Le Page, A. Sayari, Chem. Mater. 7 (1995) 1015.
[18] T.K. Das, K. Caudari, A.J. Chandwadkar, S. Sivsankar, J. Chem. Soc., Chem. Commun. (1995) 2495.
[19] K. Chaudari, T.K. Das, P.R. Rajmohanan, K. Lazar, S. Sivsankar, A.J. Chandwadkar, J. Catal. 183 (1999) 281–291.
[20] D. Zhao, D. Goldfarb, J. Chem. Soc., Chem. Commun. (1995) 875.

[21] T.D. On, M.P. Kapoor, P.N. Joshi, L. Bonneviot, S. Laliaguine, Catal. Lett. 44 (1997) 171.
[22] E. Prouzet, T.J. Pinnavaia, Angew. Chem. Int. Ed. Engl. 36 (1997) 516.
[23] S. Gontier, A. Tuel, J. Catal. 157 (1995) 124.
[24] P. Pfeifer, D. Avnir, J. Chem. Phys. 79 (1983) 3558.
[25] C.J. Brinker, G.W. Scherer. Sol–Gel Science, Academic Press, New York, 1990, p. 184.
[26] P.W. Schmidt, J. Appl. Crystallogr. 15 (1992) 567.
[27] J.E. Martin, A.J. Hurd, Scattering from fractals, J. Appl. Cryst. 20 (1987) 61–78.
[28] K.S.W. Sing, D.H. Everett, R.A.W. Haul, L. Moscou, R.A. Pierrotti, J. Rouquerol, T. Siemieniewska, Pure Appl. Chem. 57 (1985) 603.
[29] M.O. Krause, R.G. Haire, O. Keski-Rahtoken, J.R. Peterson, J. Electron Spectrosc. Relat. Phenom. 47 (1988) 215.
[30] D.J. Lam, B.W. Veal, A.P. Paulikas, ACS Symp. Ser. 216 (1983) 145.
[31] P.H. Tewari, A.B. Carnpbell, L. Colloid Interface Sci. 78 (1980) 155.
[32] T.P.M. Beelen, W.H. Dokter, H.F. van Gardren, R.A. van Santen, E. Pantos, Preparation of Catalysts, Vol. VI, Elsevier, New York, 1995, p. 33.
[33] K.F. Bradley, S.-H. Chen, P. Thiyagarajan, Phys. Rev. A 42 (1990) 6015.
[34] L. Auvray, A. Ayral, T. Dabadie, L. Cot, C. Guizard, J.D.F. Ramsey, Faraday Discuss 101 (1995) 235.
[35] K.J. Edler, P.A. Reynolds, J.W. White, D. Cookson, J. Chem. Soc., Faraday Trans. 93 (1997) 199.
[36] K.J. Edler, P.A. Reynolds, J.W. White, J. Phys. Chem. B 102 (1998) 3576.
[37] K. Aikawa, K. Kaneko, M. Fujitsu, T. Tamura, K. Ohbu, Langmuir 14 (1998) 3041.
[38] K.M. McGrath, D.M. Dabbs, N. Yao, A. Aksay, S.M. Gruner, Science 277 (1997) 552.
[39] T.P. Rieker, M.T. Anderson, P.S. Sawyer, S. Rane, G. Beaucage, in: Proceedings of the Materials Research Society Symposium, Materials Research Society, San Francisco, CA, 1998, pp. 95–99.
[40] K.J. Edler, J. Dougherty, R. Durand, L. Iton, G. Kirton, G. Lockhart, Z. Wang, R. Whithers, J.W. Smith, Colloids Surf. A: Physicochem. Eng. Aspects 1023 (1995) 213–320.
[41] A. Sayari, Chem. Mater. 8 (1996) 1840–1852.
[42] K. Kulawik, G. Schulz-Ekloff, J. Rathousky, A. Zukal, J. Had, Collect. Czech. Chem. Commun. 60 (1995) 451–456.
[43] E. Armengol, M.L. Cano, A. Corma, H. Garcia, M.T. Navarro, J. Chem. Soc., Chem. Commun. (1995) 519.